

Endoplasmic Reticulum Lipid Flux Influences Enterocyte Nuclear Morphology and Lipid-dependent Transcriptional Responses^{*,§}

Received for publication, July 20, 2016, and in revised form, September 21, 2016. Published, JBC Papers in Press, September 21, 2016, DOI 10.1074/jbc.M116.749358

Erin M. Zeituni[‡], Meredith H. Wilson[‡], Xiaobin Zheng[‡], Pablo A. Iglesias[§], Michael A. Sepanski[‡], Mahmud A. Siddiqi[‡], Jennifer L. Anderson[‡], Yixian Zheng[‡], and Steven A. Farber^{‡1}

From the [‡]Department of Embryology, Carnegie Institution for Science, Baltimore, Maryland 21218 and the [§]Department of Electrical and Computer Engineering, Johns Hopkins University, Baltimore, Maryland 21218

Edited by George Carman

Responding to a high-fat meal requires an interplay between multiple digestive tissues, sympathetic response pathways, and the gut microbiome. The epithelial enterocytes of the intestine are responsible for absorbing dietary nutrients and preparing them for circulation to distal tissues, which requires significant changes in cellular activity, including both morphological and transcriptional responses. Following a high-fat meal, we observe morphological changes in the enterocytes of larval zebrafish, including elongation of mitochondria, formation and expansion of lipid droplets, and the rapid and transient ruffling of the nuclear periphery. Dietary and pharmacological manipulation of zebrafish larvae demonstrated that these subcellular changes are specific to triglyceride absorption. The transcriptional changes that occur simultaneously with these morphological changes were determined using RNA sequencing, revealing a cohort of up-regulated genes associated with lipid droplet formation and lipid transport via lipoprotein particles. Using a microsomal triglyceride transfer protein (MTP) inhibitor to block β -lipoprotein particle formation, we demonstrate that the transcriptional response to a high-fat meal is associated with the transfer of ER triglyceride to nascent β -lipoproteins, possibly through the activation of Creb3l3/cyclic AMP-responsive element-binding protein. These data suggest that a transient increase in ER lipids is the likely mediator of the initial physiological response of intestinal enterocytes to dietary lipid.

The intestinal epithelium is largely composed of polarized, columnar, absorptive cells called enterocytes, whose apical surfaces form the lumen of the intestine (1). The plasma mem-

brane at this apical surface is characterized by a highly specialized membrane domain called the brush border and is responsible for absorbing nutrients that pass through the intestinal lumen. Enterocytes respond to the presence of food by increasing their size and remodeling several organelles, including mitochondria and the endoplasmic reticulum (ER)² (2, 3). Although a great deal is known about the structure and organization of enterocytes, many cell biological details regarding how lipids are absorbed at the apical surface, partitioned into lipid droplets within the cytoplasm, and packaged into chylomicrons for delivery to blood and lymph at the basal membrane are poorly understood.

In recent years, the zebrafish has proven to be a powerful model organism for the study of vertebrate lipid metabolism, including dietary lipid processing by the intestine and liver (4–8). Unlike *in vitro* studies, the larval zebrafish can be used to study the enterocyte response to feeding in the context of the signals and organization of the intestine *in vivo*. Dietary nutrients (e.g. lipids, proteins, and carbohydrates) can be added to zebrafish medium together with labeled lipids and/or other small molecules (9–12). In this way, a large number of larvae can be treated concurrently with different foods or pharmaceuticals, allowing for rapid and robust analyses.

The nucleus is a functionally and physically dynamic organelle that enables cells to appropriately respond to the multitude of signals required to maintain a viable multicellular organism. Between different cell types of a single organism, great diversity exists in the shape and structure of the nucleus (13). During cell division, the nucleus undergoes dramatic changes to its organization and morphology. Although the shape of the nucleus in an interphase cell is widely considered to be static, variations in nuclear shape occur in some cell types, such as neutrophils, and feature prominently in various diseases (14). Nuclear shape changes have been associated with the transduction of cytoplasmic signals into specific transcriptional responses, although many of the molecular mechanisms regulating these responses remain to be explained (15). We investigated

^{*} This work was supported in part by NIDDK, National Institutes of Health, Grants F32DK109592 (to M.H.W.) and RO1DK093399 (to S.A.F.) and NIGMS, National Institutes of Health, Grant RO1GM63904 to the Zebrafish Functional Genomics Consortium (to S. Ekker and S. A. F.). This work was also supported by the G. Harold and Leila Y. Mathers Charitable Foundation (to the laboratory of S. A. F.). The authors declare that they have no conflicts of interest with the contents of this article. The content is solely the responsibility of the authors and does not necessarily represent the official views of the National Institutes of Health.

[§] This article contains supplemental Table 1.

RNA-Seq datasets have been deposited at the NCBI GEO website (GEO Series record number GSE87704).

¹ To whom correspondence should be addressed: Dept. of Embryology, Carnegie Institution for Science, 3520 San Martin Dr., Baltimore, MD 21218. Tel.: 410-246-3072; Fax: 410-243-6311; E-mail: farber@ciwemb.edu.

² The abbreviations used are: ER, endoplasmic reticulum; RNA-seq, RNA-sequencing; apo, apolipoprotein; dpf, days postfertilization; TEM, transmission electron microscopy; COV, coefficient of variation; ANOVA, analysis of variance; TAG, triglyceride; RPKM, reads per kilobase of transcript per million mapped reads; MAG, monoglyceride; EM, embryo medium.

whether metabolic changes associated with specific dietary nutrients might play a role in nuclear morphology.

In this study, we report that when zebrafish larvae are fed a lipid-rich diet (high in triglycerides and cholesterol), the morphologies of enterocyte nuclei, mitochondria, and lipid droplets are significantly altered. The timing of these morphological changes suggests a coordination between organelles in responding to the influx of lipid. Although morphological changes in mitochondria and lipid droplets during a high-fat feed have been reported previously (2, 3, 16), here we characterize a novel rapid and reversible ruffling of the nuclear envelope that is dependent upon the absorption of dietary triglyceride. This initial observation led to a fundamental question: Does the dramatic change in nuclear morphology indicate related changes in cellular physiology?

We also report the transcriptional response of the zebrafish digestive organs to an acute high-fat feed using RNA-seq analysis and highlight the changes in gene expression involved in the synthesis, storage, and dispersal of lipids. These key physiological responses to a high-fat meal all stem from the ER, where lipids are formed and assigned to their fates. To examine the role of lipids in the ER in the enterocyte response to a high-fat meal, we disrupted the formation of key lipoprotein particles in enterocytes, the chylomicrons, using a microsomal triglyceride transfer protein (MTP) inhibitor. The MTP inhibitor blocks the lipidation of apolipoprotein B (apoB) in the ER, where it normally seeds the formation of triglyceride-loaded chylomicron particles. Inhibition of MTP led to extreme changes in nuclear morphology, probably due to the disrupted flow of lipids from the ER. Additionally, MTP inhibition reduced the transcription of key genes activated by high-fat feeding and targeted by the transcription factor Creb3l3 (cyclic AMP-responsive element-binding protein). Our hypothesis is that triglyceride within the ER induces both cellular morphological changes and transcriptional changes that reconfigure enterocytes into lipid-processing and lipid-exporting machines.

Results

A High-fat Meal Induces Changes in Enterocyte Morphology during Feeding—By 6.5 days postfertilization (dpf), zebrafish larvae have a fully functional digestive system (mouth, pharynx, intestine, liver, and pancreas), have completely absorbed their maternally deposited yolk, and actively hunt for exogenous food (17). To examine the cellular responses of the intestine in response to feeding, a lipid-rich meal was administered to the larvae for 1 h, and the intracellular morphology and organization of enterocytes were characterized at various times after the meal. Transmission electron microscopy (TEM) revealed striking morphological changes within the enterocytes, including elongation of mitochondria, appearance of cytoplasmic lipid droplets, and changes in nuclear shape (Fig. 1). As shown in Fig. 1*B*, enterocyte nuclei are initially round and smooth before feeding, but after 1 h of feeding, the shape of many enterocyte nuclei became lobular and irregular. The degree of nuclear curvature was quantified using a custom algorithm implemented in MATLAB (discussed in detail under “Experimental Procedures”). The average nuclear curvature coefficient of variation (COV) for nuclei in the unfed state was 1.12 ± 0.17 (mean \pm

S.D.), whereas this increased to 1.42 ± 0.16 following 1 h of feeding as the nuclei become ruffled (Fig. 1*D*). For each intestinal section examined, the percentage of cells exhibiting ruffled nuclei (defined as a curvature COV greater than the mean curvature COV of unfed fish plus one S.D.) also increased from an unfed baseline of $25.7 \pm 20.7\%$ to $61.6 \pm 17.0\%$ at 1 h of a high-fat meal (Fig. 1*E*). This change is transient, such that by 2 h of feeding, both the percentage of ruffled nuclei and the mean degree of nuclear curvature are similar to those in the unfed larvae (Fig. 1, *D* and *E*). There was a statistically significant difference in curvature COV and percentage of cells with nuclear ruffling between groups as determined by one-way analysis of variance (ANOVA) ($F(5,28) = 0.54$, $p < 0.0001$ and $F(5,28) = 2.81$, $p < 0.0001$, respectively). A Tukey post-hoc test revealed that both the nuclear curvature COV and the percentage of cells with nuclear ruffling at the 1-h time point were significantly higher than at all other time points and that there were no statistically significant differences between any other time points.

The timing of the ruffling of the nuclear periphery was coincident with an increase in both the population of elongated mitochondria (Fig. 1, *C* and *F*) and the appearance of lipid droplets (Fig. 1, *C* and *G*). Mitochondria also exhibited rapid changes in morphology following administration of the lipid-rich meal (Fig. 1, *C* and *F*). After the onset of feeding (30 min), the portion of mitochondria with an elongated profile grew 4-fold and maintained that level throughout the feeding time course (Fig. 1*F*).

In all cells, cytoplasmic lipid droplets are primarily composed of triglyceride (TAG) and sterol esters that can result from elevated intracellular fatty acid levels. In most cells, lipid droplets are dynamic organelles (16). In the zebrafish intestine, lipid droplets formed simultaneously with the induction of nuclear ruffling and the elongation of mitochondria (Fig. 1, *A* and *C*) and peaked in number around 1 h after feeding (Fig. 1*G*). Although the number of lipid droplets initially grew and subsequently declined, the total area occupied by lipid droplets per enterocyte remained stable over the examined time course (Fig. 1, *G* and *H*). Notably, a larger nuclear curvature COV correlates with a higher number of lipid droplets at 1 h of a high-fat feed (Pearson's $r = 0.64$, $p < 0.025$) but not with larger total area occupied by lipid droplets (Pearson's $r = 0.48$, $p < 0.10$).

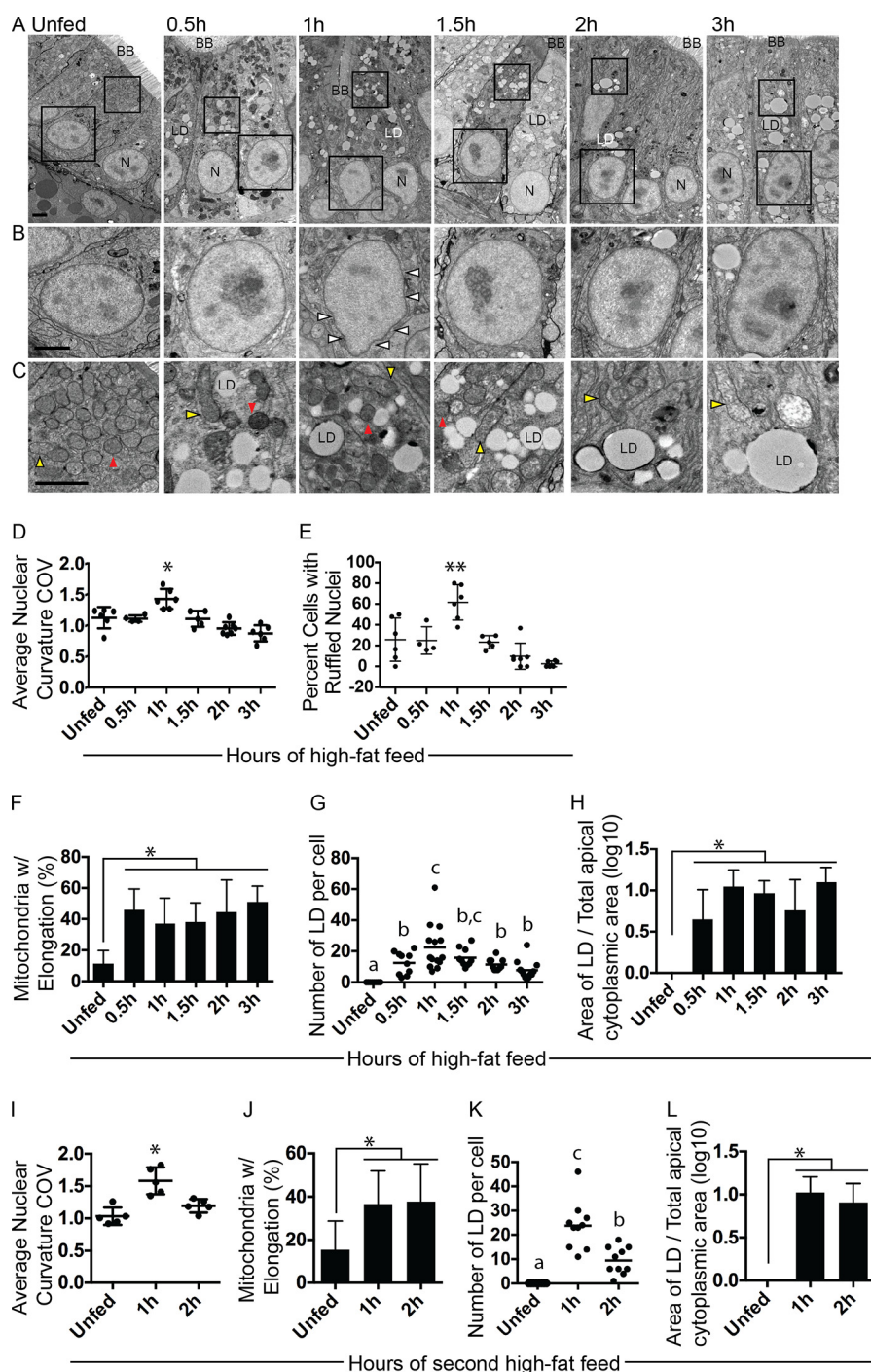
In our initial experiments, the lipid-rich meal was the first exogenous food consumed by the larvae. To evaluate the possibility that the first meal might induce cellular changes within intestinal enterocytes that are not observed in subsequent meals, 6.5-dpf larvae were fed a second, high-fat meal 24 h after being fed an initial lipid-rich meal. Following the second feeding, TEM analysis was performed at specific times informed by our “first meal” experiment (Fig. 1, *I–L*). Similar to the response observed after the first meal, the shape of enterocyte nuclei exhibited a transient increase in the degree of curvature 1 h after feeding (Fig. 1*I*). Furthermore, changes in mitochondrial shape and lipid droplet number during the second high-fat meal matched both the timing and the profile of the initial high-fat meal (Fig. 1, compare *F* and *G* with *J* and *K*). Additional examination of older zebrafish larvae, fasted for 24 h at 14 dpf and fed a high-fat meal at 15 dpf, also demonstrated a robust

ER Lipid Activities: Morphological and Transcriptional Responses

induction of these subcellular changes in response to a high-fat meal (data not shown).

Enterocyte Nuclear Ruffling Is Induced Specifically by Meals That Include Fat—To determine whether the observed changes in nuclear morphology are specific to absorption of dietary fat, meals of different nutrient composition were fed to the larvae (6.5 dpf), followed by TEM analysis. Our data indicate that only lipid-rich foods were able to induce nuclear ruffling (Fig. 2, A and B; one-way ANOVA ($F(4,38) = 2.30, p < 0.0001$). A Tukey post-hoc test revealed chicken egg yolk and artemia feeds induced a statistically significant increase in nuclear curvature

COV. This ruffling followed the same reversible profile observed previously, so that at 2 h after the initiation of feeding, nuclei returned to an unruffled state in both chicken egg yolk and artemia (data not shown). The higher amount of fat in chicken egg yolk solution (1.3% lipid (w/v)) increased the proportion of enterocytes exhibiting ruffled nuclei, as compared with what was observed in fish fed artemia solution (0.5% lipid (w/v)) (Fig. 2C), suggesting that there may be a threshold level of lipid in the cell that must be reached before ruffling is observed. Food solutions that contained little fat (spirulina, 0.002% lipid (w/v)) or no fat (chicken egg white and glucose) did



not induce nuclear ruffling. In these low-fat or fat-free conditions, nuclear ruffling was not simply delayed, because no evidence of ruffling was observed at 2 h after feeding was initiated (data not shown). As expected, lipid droplet formation was only observed in the chicken egg yolk- and artemia-fed fish (Fig. 2A). However, the appearance of the lipid droplets was remarkably different in animals fed these two foods; lipid droplets in the egg yolk-fed larvae were less electron-dense than those in the artemia-fed fish. Given that a major site of osmium reactivity is the C=C double bonds contained within the acyl chains of complex lipids (18), the darker osmium stain observed in artemia lipid droplets would suggest a higher number of polyunsaturated acyl chains than egg yolk. In fact, egg yolk acyl chains are predominantly monounsaturated fatty acids (42% oleic, 18:1) and saturated fatty acids (28% palmitic, 16:0; 9% stearic, 18:0) (19), whereas artemia contains 28% polyunsaturated fatty acids in addition to 52% monounsaturated fatty acids (20).

Pharmaceutical Manipulation of Dietary Lipid Absorption Links Triglyceride Metabolites (Monoglyceride/Free Fatty Acid) to Nuclear Ruffling—Egg yolk is composed of a heterogeneous mixture of lipids that includes phospholipids, cholesterol, and TAG (21, 22). To determine whether a particular lipid constituent was inducing changes in nuclear morphology, we treated larvae with pharmaceutical drugs that inhibited the uptake of cholesterol or TAG metabolites in conjunction with the previously described high-lipid meal (Fig. 2D). To test the hypothesis that dietary cholesterol was mediating nuclear ruffling, cholesterol absorption was blocked pharmacologically using the Npc1l1 inhibitor ezetimibe (23–25). Consistent with previous studies (11, 26), ezetimibe treatment efficiently inhibited the uptake of fluorescent cholesterol analog (TopFluor-Cholesterol, Avanti Polar Lipids) into the enterocytes of treated animals (data not shown). Importantly, ezetimibe treatment had no effect on feeding (data not shown). Notably, zebrafish treated with ezetimibe before a high-fat meal formed intestinal cytoplasmic lipid droplets similarly to their untreated and vehi-

cle-treated counterparts (Fig. 2F). However, nuclear ruffling was no different in degree or timing from the untreated and vehicle-treated controls (Fig. 2E), indicating that dietary cholesterol is not responsible for the observed nuclear ruffling.

To evaluate the role of TAG byproducts produced in the intestinal lumen following a high-fat meal, orlistat was utilized to prevent the action of pancreatic lipases, which subsequently blocks enterocyte absorption of TAG metabolites of triglycerides (fatty acids and monoglycerides) and cholesterol esters (27). As was the case with ezetimibe, orlistat did not alter the total amount of food consumed (data not shown). As evidence of the drug's effectiveness in the larval zebrafish, treated animals failed to form cytoplasmic lipid droplets (Fig. 2F), due to a lack of absorbed fatty acids required for the synthesis of TAG within the ER and the subsequent formation of cytoplasmic lipid droplets (28). Furthermore, orlistat-treated fish exhibited attenuated nuclear ruffling, suggesting that monoglycerides/free fatty acids are the dietary trigger that induces nuclear ruffling (Fig. 2E).

A High-fat Meal Alters the Transcription of Genes Involved in Lipid Transport, Storage, and Metabolism—The morphological changes observed in enterocytes are indicative of a rapid and robust cellular response to an influx of dietary fatty acids and other TAG metabolites. As the cell exits a resting state, transcriptional changes must occur that allow for the enterocyte to up-regulate lipid export through lipoprotein particle secretion as well as intracellular lipid storage capacity (29). The rapid morphological responses observed in our studies indicated that an early time point (1 h postfeeding) would capture the initial cellular response to dietary fat. We performed RNA-seq analysis of zebrafish larval (6.5 dpf) gut RNA from animals fed with either chicken egg white or egg yolk (1 and 4 h postmeal) to identify genes that were specifically changed by a high-fat meal and not by feeding. In addition, we performed RNA-seq with 6.5-dpf zebrafish guts before feeding (unfed controls) as a reference. The results of three separate experiments were utilized to compare the induction or repression of transcripts under

FIGURE 1. A high-fat meal induces changes in enterocyte morphology during feeding. *A*, time course of 6.5-dpf zebrafish larvae fed a high-fat meal composed of an emulsion of 5% chicken egg yolk. Electron micrographs show representative images of cellular changes in intestinal epithelial cells before feeding (unfed) and at 0.5, 1, 1.5, 2, and 3 h after feeding begins. *N*, nucleus; *LD*, lipid droplet; *BB*, brush border. *B*, enlargement of enterocyte nuclei (boxed) at the indicated time points of a high-fat meal. Nuclear ruffling is indicated by white arrowheads. *C*, enlargement of a portion of apical cytoplasm (boxed) of enterocytes at given time points of a high-fat meal. Examples of rounded and elongated mitochondria are indicated with red and yellow arrowheads, respectively. *D*, quantification of the average curvature COV of nuclei at each time point. Each dot represents an average of ≥ 10 nuclei from a single fish. There was a statistically significant difference between groups as determined by one-way ANOVA ($F(5,28) = 0.54$, $p < 0.0001$). A Tukey post-hoc test revealed that the curvature COV at the 1 h time point was statistically significantly higher than all other time points and that there were no statistically significant differences between any other time points. *E*, quantification of the percentage of cells exhibiting ruffled nuclei at each time point. Each dot represents an average of ≥ 10 nuclei from a single fish. There was a statistically significant difference between groups as determined by one-way ANOVA ($F(5,28) = 2.81$, $p < 0.0001$). A Tukey post-hoc test revealed that the percentage of cells with ruffled nuclei at the 1 h time point was statistically significantly higher than at all other time points and that there were no statistically significant differences between any other time points. *F*, quantification of the frequency of elongated mitochondria at each time point. Two cells from each fish were analyzed. There was a statistically significant difference between groups as determined by one-way ANOVA ($F(5,64) = 1.56$, $p < 0.0001$). A Tukey post-hoc test revealed that mitochondrial elongations at the 0 h time point were statistically significantly lower than at all other time points and that there were no statistically significant differences between any other time points. *G*, quantification of the number of lipid droplets per cell at each time point. Each dot represents the number of lipid droplets in a single cell; two cells were analyzed per fish. There was a statistically significant difference between groups as determined by one-way ANOVA ($F(5,62) = 4.01$, $p < 0.0001$). A Tukey post-hoc test revealed that the number of lipid droplets increased significantly within 30 min of eating a high-fat meal, peaking at 1 h and then decreasing with time. *H*, quantification of the portion of the apical cytoplasmic area that is composed of lipid droplets at each time point. Two cells from each fish were analyzed. Log₁₀ adjustment was used to reduce the effect of outliers. There was a statistically significant difference between groups as determined by one-way ANOVA ($F(5,64) = 3.60$, $p < 0.0001$). A Tukey post-hoc test revealed that the portion of the total apical cytoplasmic area taken up by lipid droplets increased significantly upon feeding but did not change as the high-fat feeding time course progressed, so that the lipid droplet area at 1 h postfeeding was not statistically significantly different from the lipid droplet area at 3 h postfeeding. *I–L*, quantification of subcellular changes observed in intestinal epithelial cells before refeeding (unfed) and at 1 and 2 h after the refeeding began. Measured changes include curvature COV of enterocyte nuclei (*I*), morphology of mitochondria (*J*), and lipid droplet number and size (*K* and *L*, respectively). Quantification protocols match those used in *C*, *E*, *F*, and *G*. Statistically significant differences between groups were determined by one-way ANOVA with a Tukey post-hoc test for multiple comparisons. Similar trends were observed in both the first (*A–H*) and second (*I–L*) high-fat feedings. Error bars, S.D.

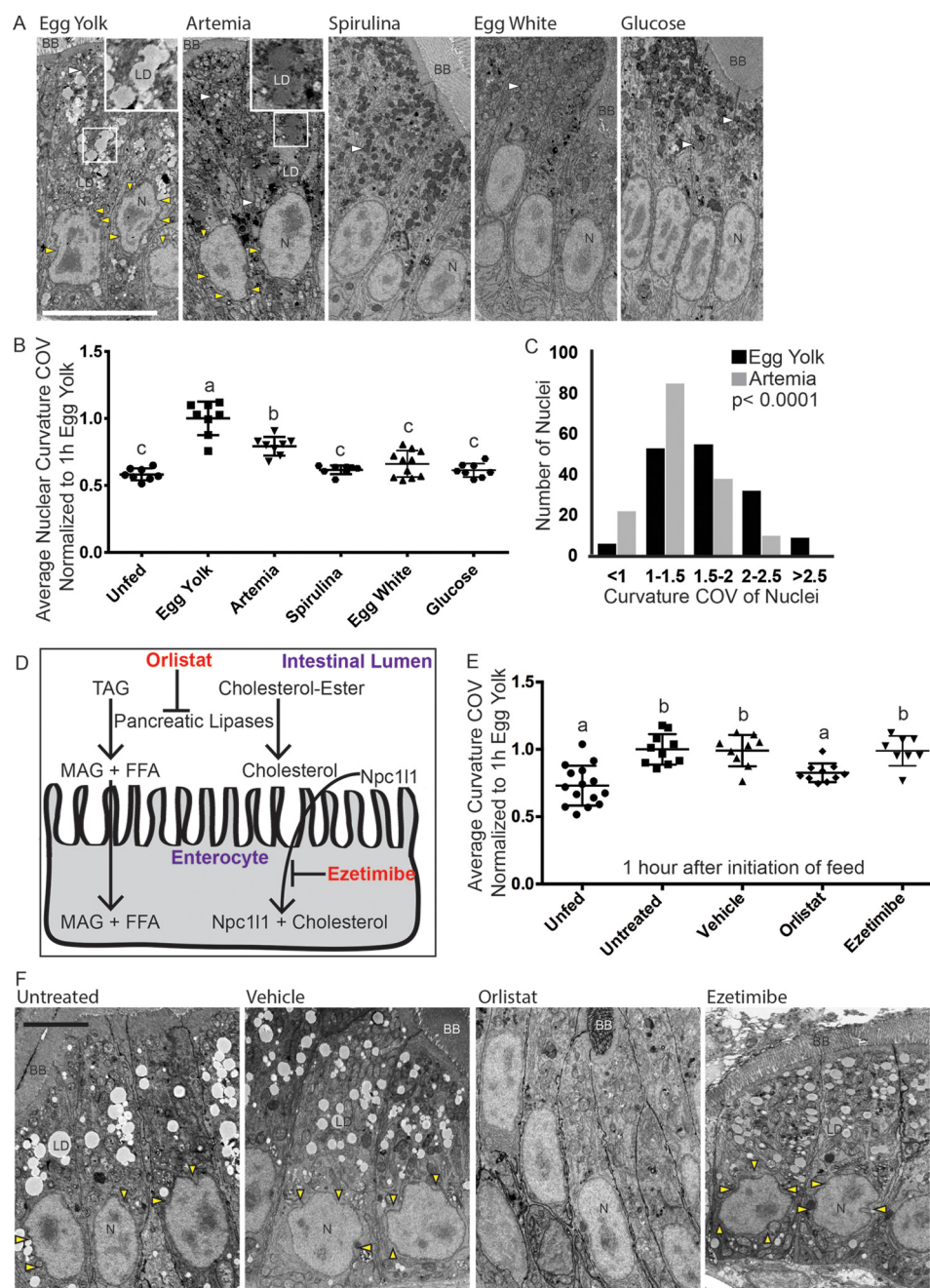


FIGURE 2. Lipid metabolites trigger enterocyte nuclear ruffling and lipid droplet production. *A*, time courses of 6.5-dpf zebrafish larvae fed various diets. Electron micrographs show representative images of cellular changes in enterocytes at 1 h after feeding began. *N*, nucleus; *LD*, lipid droplet; *BB*, brush border. *Yellow arrowheads* indicate nuclear ruffling. *White arrowheads* indicate mitochondria. *Scale bar*, 10 μ m. *Inserts* highlight differences in lipid droplets between egg yolk and artemia-fed larvae. *B*, quantification of nuclear curvature COV observed in intestinal epithelial cells at 1 h after initiation of feeding of the indicated food. Each dot represents an average of at least 10 nuclei from a single fish. Curvature COV measurements were normalized to 1-h egg yolk feed. Statistical analysis was conducted with the raw data. There was a statistically significant difference between groups as determined by one-way ANOVA ($F(4,38) = 2.30$, $p < 0.0001$). A Tukey post-hoc test revealed that egg yolk and artemia feeds induced a statistically significant increase in nuclear curvature COV. In contrast, spirulina, egg white, and glucose feeds exhibited nuclear curvature COV similar to the unfed control. *C*, analysis of the profile of curvature COV of enterocyte nuclei from fish fed egg yolk or artemia solutions. Nuclei were binned based on their curvature COV measurement. 155 nuclei were analyzed and graphed for each condition. χ^2 analysis demonstrates a significant difference in the nuclear ruffling between the two treatment groups ($p < 0.0001$). *D*, schematic mode of action of drugs that block dietary lipid absorption by enterocytes. *E*, quantification of nuclear curvature COV observed in treated intestinal epithelial cells at 1 h of a high-fat meal. Each dot represents an average of at least 10 nuclei from a single fish. Curvature COV measurements were normalized to untreated larvae at 1 h of a high-fat meal. Statistical analysis was conducted with the raw data. There was a statistically significant difference between groups as determined by one-way ANOVA ($F(7,74) = 1.07$, $p < 0.0001$). A Tukey post-hoc test revealed a significant increase in nuclear curvature COV in the untreated, vehicle-treated, and ezetimibe-treated fish. In contrast, fish treated with orlistat exhibited nuclear curvature COV similar to the unfed control. *F*, 6.5-dpf zebrafish larvae treated with vehicle, orlistat, or ezetimibe and fed a high-fat meal for 1 h. Electron micrographs show representative images of cellular changes in enterocytes from the indicated treatment groups at 1 h after feeding began. *Yellow arrowheads* indicate nuclear ruffling. *Scale bar*, 10 μ m. *Error bars*, S.D.

ER Lipid Activities: Morphological and Transcriptional Responses

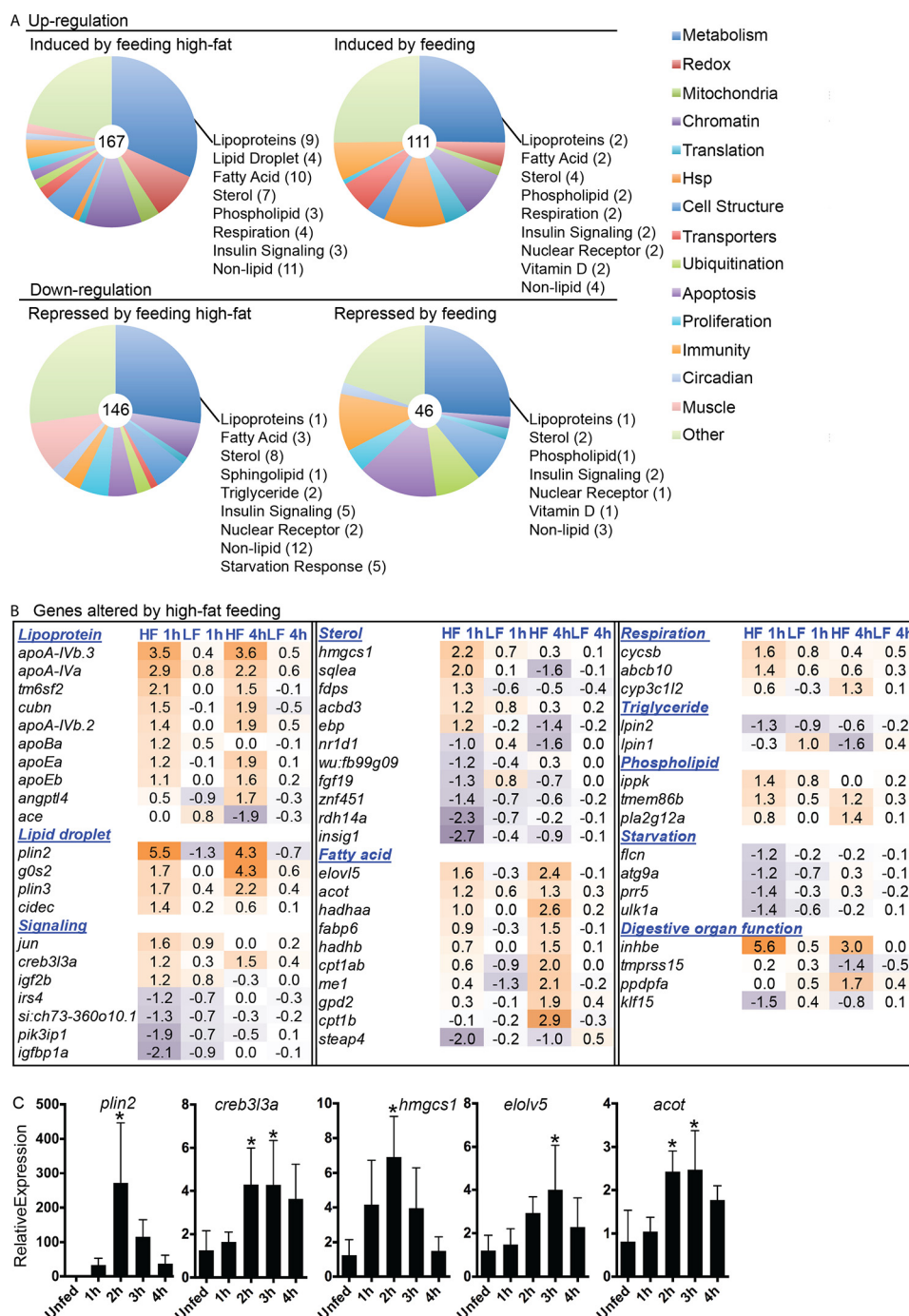


FIGURE 3. A high-fat meal induces a unique transcriptional response. A, overview of the genes induced in larval guts upon feeding 6.5-dpf zebrafish a high-fat and a fat-free meal, as assayed by RNA-seq. Samples were taken before feeding (unfed) and at 1 and 4 h after feeding began. The transcript reads from unfed fish were treated as the baseline for each group. The total number of genes whose expression changed only with a high-fat diet (*Induced/Repressed by feeding high-fat*) or with both types of food (*Induced/Repressed by feeding*) are indicated in the center of the diagrams. Genes are grouped by function. B, gene families with a role in metabolism that were specifically induced or repressed by a high-fat meal are shown. The table indicates the -fold change of expression (log₂) over unfed controls, as determined by RNA-seq analysis. The table is color-coded to indicate induction (orange) or repression (purple). Statistical analysis of the -fold changes for each condition are shown in supplemental Table 1. C, RT-PCR validation of high-fat meal induction of the most robustly changed genes from several gene categories involved in lipid storage and metabolism. Relative expression is shown, normalized to an unfed control for each respective treatment using the $\Delta\Delta C_T$ method. There was a statistically significant difference between groups as determined by one-way ANOVA (*plin2* ($F(4,15) = 17.50$, $p < 0.002$; *creb3l3a* ($F(4,15) = 2.49$, $p < 0.02$; *hmgcs1* ($F(4,15) = 2.32$, $p < 0.006$; *elovl5* ($F(4,15) = 3.67$, $p < 0.04$; *acot* ($F(4,15) = 0.42$, $p < 0.006$). Dunnett's post-hoc test revealed significant differences between unfed controls and certain time points of a high-fat feed. Time points with a statistically significant increase in expression over unfed controls are indicated by an asterisk. Error bars, S.D.

each condition and at specific time points (unfed controls were used to determine baseline transcription levels) (supplemental Table 1). This allowed us to separate genes induced or repressed specifically by high-fat meals from those that were

induced or repressed by feeding in general (Fig. 3A). Conclusions based on RNA-seq data must be determined by a combined examination of -fold change and reads per kilobase of transcript per million mapped reads (RPKM) of genes of inter-

est (supplemental Table 1). -Fold changes presented are on a log₂ scale, and significant -fold changes ($p < 0.05$) between 1.0 and -1.0 were excluded from the analysis. RPKMs <3.4 (2 times the highest RPKM value of *nanos* (1.73) across the three experimental groups) were considered artifacts and excluded as well.

As expected, the expression of genes involved in metabolism, chromatin organization, translation, cellular structure, proliferation, and immunity were altered regardless of the type of food (Fig. 3A). Examination of the genes specifically up-regulated by high-fat feeding revealed an enrichment in lipoprotein synthesis and transport genes (*apoA-IVb.3*, *apoA-IVa*, *tm6sf2*, *cubn*, *apoA-IVb.2*, *apoBa*, *apoEa*, *apoEb*, and *angptl4*), lipid droplet synthesis and maintenance (*plin2*, *g0s2*, *plin3*, and *cidec*), and sterol and fatty acid processing (*hmgcs1*, *elovl5*, *acot*, *splea*, *fdps*, *acbd3*, and *ebp*) (Fig. 3B). Genes involved in sterol and triglyceride synthesis (*nr1d1*, *fgf19*, *znf451*, *rdh14a*, and *insig1*) as well as genes involved in the response to starvation (*flcn*, *atg9a*, *prf5*, and *ulk1a*) were largely down-regulated, consistent with the consumption of food rich in fat and cholesterol. The high-fat expression pattern of apolipoprotein transcription during these early time points is consistent with results published previously (30). The genes most robustly up-regulated in response to the high-fat meal are involved in apolipoprotein synthesis, lipid droplet processing (*plin2*), triglyceride signaling (*creb3l3a*), sterol metabolism (*hmgcs1*), and fatty acid metabolism (*elovl5* and *acot*). These transcriptional increases were verified by quantitative RT-PCR (Fig. 3C). Many of these highly up-regulated genes (*hmgcs1*, *elovl5*, *creb3l3a*, *insig1*, and *apoBa*) localize to the ER, where absorbed lipid metabolites are targeted for processing, storage, and export.

Inhibition of ER Lipid Flux Increases Nuclear Ruffling and Attenuates the Transcriptional Response to a High-fat Meal—The RNA-seq and TEM results both demonstrate a rapid and robust shift in enterocyte morphology and physiology in response to dietary fatty acids. Specifically, the enterocyte increases its propensity for lipid storage (TAG synthesis and lipid droplet synthesis) and export (lipoprotein synthesis). Both of these processes start at the smooth ER, where fatty acids are incorporated into TAG within the ER membrane bilayer (Fig. 4C). ER TAG can then either bud off to form lipid droplets or bind MTP for transfer to apoB and subsequent secretion within a mature lipoprotein (29). Chylomicron secretion is regulated primarily by lipid availability in the ER for lipoparticle assembly, a process initiated when MTP offloads its TAG to apoB as it is passing through the ER translocon (31). To explore the specific role of ER TAG on the morphological and transcriptional changes observed in enterocytes, an inhibitor of MTP (lomitapide) (32, 33) was administered to block both lipoprotein synthesis and ER TAG flux. Our data indicate that disrupting these critical enterocyte functions enhanced and prolonged the degree of nuclear curvature (Fig. 4, A–C). Notably, nuclear ruffling has not been observed in cells of other digestive organs known to produce lipoprotein particles (such as the liver) under any feeding conditions. Although treatment with the MTP inhibitor did not alter MTP gene expression, it did reduce the responsive expression of a large number of genes important for apolipoprotein synthesis (Fig. 4D). MTP inhibition also dampened the responsive expression of

plin2 and *hmgcs1*, key regulators of lipid droplets and TAG processing, respectively (Fig. 4D).

Discussion

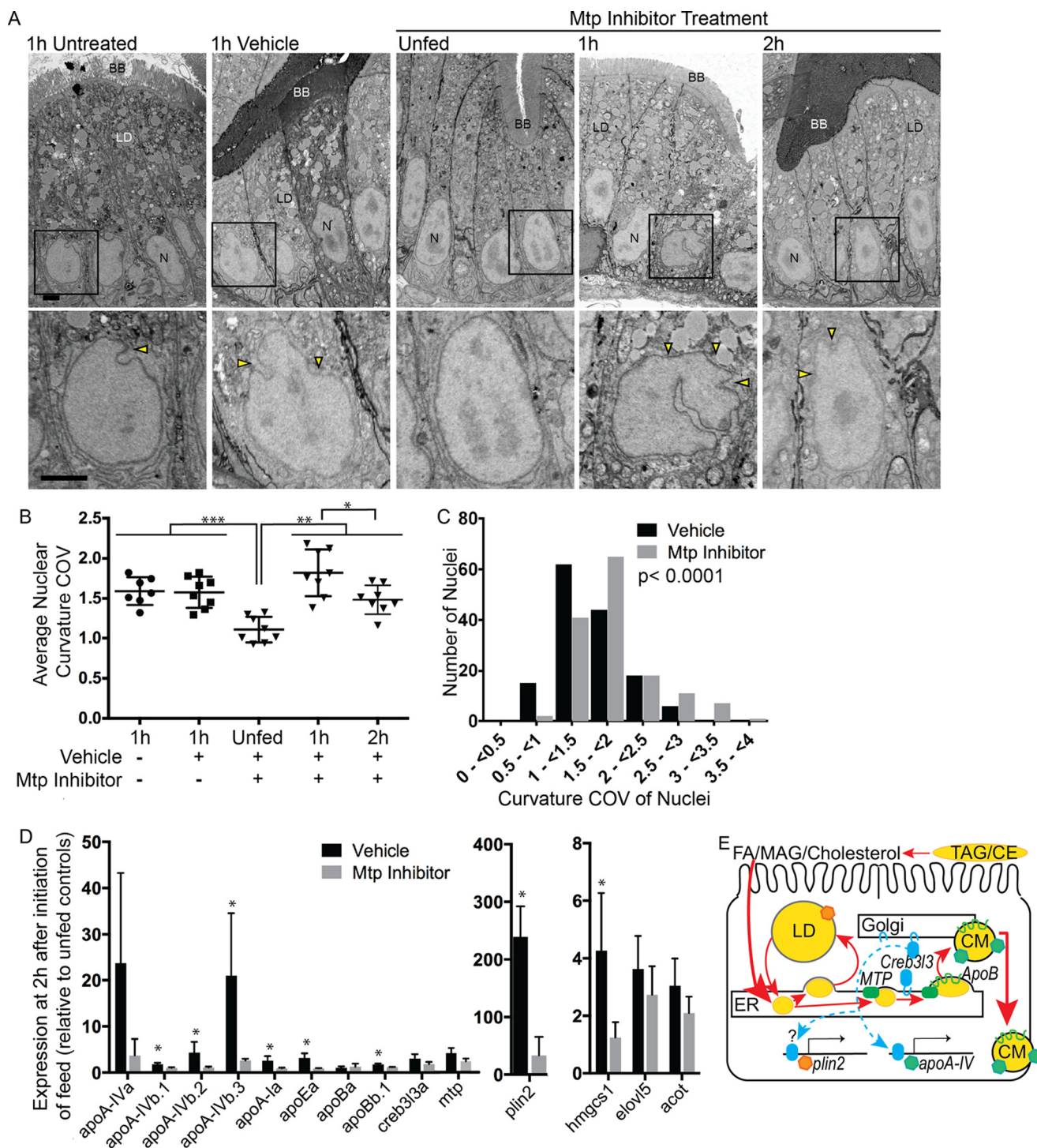
Dramatic morphological changes of the nucleus, mitochondria, and lipid droplets are induced by a high-fat meal. TEM has been a mainstay approach to visually examining fat absorption, transport, and packaging in the intestine because of the ease with which lipid droplets can be detected (34). Classical ultrastructural studies examining the effect of feeding on mammalian enterocyte subcellular structures are consistent with our observations in zebrafish larvae. Several prior studies have described the effect of an oil gavage on rodent enterocyte morphology (increases in lipid droplets and expansion of smooth endoplasmic reticulum and Golgi) (34–36). Although few authors comment on nuclear morphology in these studies, a reexamination of these TEM images clearly reveals the unique nuclear ruffling of enterocytes. Buschman and Manke (2, 3) compared the ruffling of the enterocyte nuclei in fasted and fat-fed hamster by subjective examination of the overlay of traced nuclei. They determined that high-fat feeding does indeed alter the peripheral ruffling of the nucleus, although they observed nuclear ruffling in both fed and unfed states. Modest nuclear ruffling was also observed in the enterocytes of 1.5-year-old zebrafish adults after a 90-h fast (data not shown). We predict that the discrepancy between nuclear ruffling in fasted adults and larvae may be due to developmental differences in the intestine combined with the absence of adipose tissue in 6.5-dpf zebrafish larvae. Adults have stored lipids in their adipose tissue that can be used to elevate circulating free fatty acids in the fasted state, whereas larvae would require lipid synthesis or metabolism to acquire new lipids in the absence of dietary lipid. The absence of fat tissue may amplify the physiological and morphological responses in larval enterocytes to dietary lipid. Further examination of the enterocyte response to high-fat feeding at different ages in zebrafish will determine the effect of age and adipocyte lipid storage.

Although the cause of the robust and rapidly reversible nuclear ruffling described here is still unclear, we hypothesize that the initial influx of dietary fat may transiently increase lipids in the ER and associated nuclear envelope, thereby altering the rigidity of the nuclear membrane. As the cell up-regulates lipid export and storage, ER lipid homeostasis may be restored along with nuclear curvature. The ruffling of the nuclear periphery might also indicate dramatic modifications and reorganization of the nuclear lamina and associated chromatin. This reorganization could prepare the cell to exit a resting state and enter into a state of high metabolic, storage, and export activity.

Within 30 min of feeding a high-fat meal, a robust morphological response of mitochondrial elongation was observed. Alterations in mitochondrial morphology were previously noted by Jasper and Bronk (37) in rat mucosal strips exposed to exogenous amino acids. Furthermore, mitochondrial fusion can be promoted by increased metabolic demand (38). The dramatic shifts in mitochondrial morphology observed here in the larval zebrafish intestine are consistent with enhanced fusion driven by the metabolic demands of rapid lipid influx.

The correlation between the number of lipid droplets and the degree of nuclear ruffling at 1 h of a high-fat meal suggests a connection between the nucleus, lipid droplets, and the ER that plays a predominant role in early lipid droplet formation. Upon high-fat feeding, lipid droplets form and subsequently expand, so that the number of lipid droplets starts to decline at 2 h postfeeding, whereas the total area occupied by lipid droplets remains stable to 3 h. One possible hypothesis is that small lipid droplets initially form throughout the cytoplasm, grow, and then fuse to form larger lipid droplets. Although no direct

observations of fusion events were noted, these data are consistent with a prior study in cultured cells where 15% of all lipid droplets are engaged in fusion events at any given moment (39). These data are also consistent with a model of two pools of lipid droplets: one with enzymes that synthesize TAG and the other associated with lipases that result in TAG loss. Assuming that the cell is absorbing fatty acids/monoglyceride (MAG) at a steady rate, the stability of enterocyte lipid droplet area can be explained by a shift in the enterocyte's physiology to drive lipid export (through lipo-



protein synthesis and secretion) and to promote lipid oxidation.

The timing and profile of the nuclear, mitochondrial, and lipid droplet morphological changes of a second high-fat feed closely mirrored morphological changes in the initial high-fat meal. Therefore, these morphological responses are not simply a consequence of the first exposure of the intestine to exogenous food but are more likely a typical enterocyte response to high-fat feeding in larvae.

By manipulating the amount of lipid absorbed by enterocytes after a meal by altering the diet, we identified the meal's lipid content as a key indicator of nuclear ruffling. Meals that did not contain lipid (glucose and egg white solutions) did not induce nuclear ruffling or lipid droplet formation. For meals that did contain lipid (egg yolk, artemia, and spirulina solutions), there appeared to be a threshold level of lipid absorption that must be reached before ruffling and lipid droplets are observed. For example, no nuclear ruffling was observed in spirulina-fed fish (0.002% lipid (w/v)), but nuclear ruffling was observed in both larvae fed egg yolk solution (1.3% lipid (w/v)) and artemia solution (0.5% lipid (w/v)). Further, the proportion of enterocytes exhibiting ruffled nuclei was higher in larvae fed chicken egg yolk solution than in larvae fed artemia solution. Future examination of the total lipid content of enterocytes after meals with various levels of lipid would provide more insight into this possible explanation.

Pharmaceutical manipulation of dietary lipid absorption linked triglyceride metabolites in particular to nuclear ruffling. Blocking the absorption of dietary cholesterol with ezetimibe treatment before a high-fat meal had no effect on the timing or magnitude of nuclear ruffling and lipid droplet formation. However, blocking the absorption of dietary monoglycerides and free fatty acids using orlistat attenuated nuclear ruffling and lipid droplet formation. Therefore, the same high-fat egg solution capable of inducing rapid and robust morphological changes in enterocytes cannot induce a response when treated with orlistat. We hypothesize that the acute lipid flux within the ER resulting from monoglyceride/fatty acid absorption and subsequent ER TAG synthesis 1) plays a role in altering the nuclear periphery, which results in a ruffled nuclear appearance, or 2) induces a reorganization of the nuclear periphery as the cell transitions from a resting state (fasted) to a transcriptionally responsive state (fed), which results in a ruffling of the nuclear periphery.

The transcriptional profile of enterocytes rapidly responds to a high-fat meal, with changes in gene expression occurring as early as 1 h after feeding. Genes involved in lipid transport, storage, signaling, and metabolism were most responsive to a high-fat meal. This change in transcriptional profile indicates that under high-fat feeding conditions, regulation of lipid is paramount to the enterocyte response. Specifically, the enterocyte increases its propensity for lipid storage (TAG synthesis and lipid droplet synthesis) and export (lipoprotein synthesis), probably both to protect the enterocytes from the toxic effects of free fatty acids and to ensure that dietary lipids are distributed throughout the body.

Analysis of the genes whose expression changed in response to a high-fat meal indicates the activity of multiple lipid-induced signaling proteins (insulin, *ppar-γ*, *srebp*, and *creb3l3*) and pathways, which converge on the ER as absorbed lipid metabolites are targeted to this organelle. Future work examining the interplay between these pathways in the intestine would enhance fields largely focused on the function of these pathways in other metabolic tissues (*i.e.* the liver).

Among the highest up-regulated genes, the enrichment of ER-localized genes involved in lipid processing, signaling, and export indicated a critical role of this organelle in the enterocyte response to absorbed dietary lipid. Pharmaceutical inhibition of ER lipid packaging into apolipoproteins using an MTP inhibitor enhanced the magnitude and duration of nuclear ruffling. The increased nuclear ruffling seen when lipoprotein synthesis and export are blocked is consistent with our hypothesis that increased levels of lipid in the ER result in changes to the rigidity of the nuclear envelope. The presumptive increase of TAG within the ER caused by blocking lipid transport through chylomicrons could be responsible for this increased level of nuclear ruffling. These data are consistent with reports from humans with abetalipoproteinemia and mice with MTP deficiency showing slightly more ruffled nuclei as compared with control (40, 41). However, few of the published electron micrograph images include enterocyte nuclei, making it difficult to draw definitive conclusions as to the effect of lipoprotein retention on mammalian enterocyte nuclear morphology.

Nuclear ruffling has not been observed in cells of other digestive organs known to produce lipoprotein particles (such as the liver) under any feeding conditions. The unique rapid influx of lipid to the intestinal lumen and subsequently to the enterocytes may have a stronger effect on nuclear morphology than

FIGURE 4. Treatment with an MTP inhibitor alters the enterocyte response to a high-fat meal. *A*, representative electron micrographs of 6.5-dpf untreated zebrafish larvae and larvae treated with vehicle or MTP inhibitor and fed a high-fat meal indicating cellular changes in enterocytes as a result of treatment. Yellow arrowheads indicate nuclear ruffling. Scale bar, 2 μ m. *B*, quantification of nuclear curvature COV observed in the TEM experiment. Each dot represents an average of at least 10 nuclei from a single fish. There was a statistically significant difference between groups as determined by one-way ANOVA ($F(4,34) = 1.08$, $p < 0.0001$). A Tukey post-hoc test revealed a statistically significant increase in nuclear curvature COV in all fed treatment groups, when compared with the MTP inhibitor-treated unfed control. The increased nuclear curvature COV observed with feeding MTP inhibitor-treated fish was significantly higher at 1 h and was maintained at least 2 h into the time course. *C*, analysis of the profile of curvature COV of enterocyte nuclei from fish treated with vehicle or with MTP inhibitor. Nuclei were binned based on their curvature COV measurement. 145 nuclei were analyzed and graphed for each condition. χ^2 analysis demonstrates a significant difference between the nuclear ruffling of the two treatment groups ($p < 0.0001$). *D*, RT-PCR of cDNA extracted from 6.5-dpf zebrafish guts dissected at 2 h after feeding a high-fat meal with either vehicle treatment or MTP inhibitor treatment. Relative expression is shown, normalized to an unfed control for each respective treatment using the $\Delta\Delta C_T$ method. Statistical analysis was conducted using the unpaired Student *t* test to identify differences between vehicle-treated and MTP inhibitor-treated groups. *, $p < 0.05$. *E*, schematic of lipid flux in the enterocyte after a high-fat meal. TAG is broken down into fatty acids (FA) and monoglyceride in the intestinal lumen. These metabolites are then absorbed by enterocytes and reconstituted into TAG in the ER, where it has two primary fates: 1) packaging into lipid droplets for short term storage (<16 h) or 2) incorporation into apoB- and apoA-IV-labeled chylomicrons (CM) for export to distal tissues. Creb3l3 is activated by a high-fat meal, leading to its transport from the ER to the Golgi, where it is cleaved and translocated into the nucleus to serve as a transcription factor. We hypothesize that the TAG lipidation and translocation of apoB may serve as the activating signal that triggers the movement of Creb3l3 from the ER to the Golgi. CE, cholesterol ester; Error bars, S.D.

the gradual change in lipid flux experienced by other tissues. Future intestinal studies will clarify this potential connection between lipid flux in the ER and changes to the structure and/or organization of the nuclear periphery.

Notably, genes that had responded to the acute high-fat meal but were dampened by MTP inhibitor treatment, such as apoA-IV, closely mirror the affected genes identified in longer term atherogenic feeding studies in mice lacking the Creb3l3 transcription factor, a member of the CREB3 (cyclic AMP-responsive element-binding protein) family of bZIP transcription factors (42). Further, Creb3l3 knock-out mice fasted for 24 h show a similar misregulation of genes involved in lipid transport and triglyceride metabolism in both liver and intestine (43). Creb3l3 is an ER-tethered transcription factor activated by saturated fatty acids, insulin, and/or inflammatory stimuli whose expression is restricted to the liver and intestine of vertebrates, including zebrafish (42, 44–46). Prior studies have demonstrated that Creb3l3 strongly up-regulates apoA-IV, a gene that is primarily expressed in the intestine (30), where it can expand chylomicron size to increase gross lipid export (47–51). Zebrafish have multiple apoA-IV genes that exhibit rapid increase in expression in the intestine after high-fat feeding (Fig. 3B) (30). We propose that the reduction in apoA-IV expression that we observe under MTP inhibition is due to a reduction in Creb3l3 processing and activity, as observed by Cheng *et al.* (52). Cheng *et al.* (52) show that TAG flux in the hepatocyte ER controls apoB-VLDL particle assembly, which regulates Creb3l3 proteolytic processing, which in turn promotes the up-regulation of apoA-IV expression to enhance the efficient export of lipid (52). In our hands, MTP inhibition also dampened the responsive expression of *plin2* and *hmgs1*, key regulators of lipid droplets and TAG processing, respectively (Fig. 4D). Taken together, these findings support our hypothesis that TAG flux in the enterocyte ER stimulates a robust cellular response that coordinates lipid processing, storage, and export from the cell.

Experimental Procedures

Zebrafish—All procedures were approved by the Carnegie Institution Animal Care and Use Committee (protocol 139). For all experiments, WT (AB background) embryos were collected from natural spawning, staged, and raised in zebrafish embryo medium (EM) as described previously (53).

Preparation of Zebrafish Meals—For all feeding solutions, a total volume of 20 ml was prepared. The high-fat vesicle feeding solution was prepared similarly to previous reports (12, 54). Briefly, a 5% egg yolk emulsion was made with frozen aliquots of chicken egg yolk resuspended in zebrafish EM. The egg yolk emulsion was pulse-sonicated (Sonicator Ultrasonic Processor 6000, Misonix Inc.) for 10 s using a ¼-inch tapered microtip (output intensity, 3 W; 1 s on/off; 5-s total processing time), passed through a strainer, pulse-sonicated for an additional 30 s, and then vortexed for 30 s. The artemia feed was prepared as 1% (w/v) shell-free artemia (INVE Aquaculture) in zebrafish EM and sonicated for 5 s for uniformity. The spirulina solution was prepared as 0.5% (w/v) spirulina powder (Salt Creek Inc.) in EM and mixed by vortexing. The glucose solution was prepared as 5% (w/v) glucose in EM and mixed by vortexing. A 10% egg

white solution was made with frozen aliquots of chicken egg white resuspended in EM and sonicated for 5 s.

Feeding Zebrafish—To improve feeding rates, all feeding assays were performed in 35-mm Petri dishes kept in an incubated orbital shaker set to 29 °C and 30 rpm (Incu-Shaker Mini H1000-M, Benchmark Scientific). For assays measuring transcriptional responses to feeding, 30–40 larvae were placed in 5 ml of sonicated egg yolk emulsion to feed. For TEM experiments, 70–100 larvae were placed in 5 ml of sonicated egg yolk emulsion to feed. For all feeding procedures, after 50 min in the feeding solution, larvae were washed two times in embryo medium, anesthetized with tricaine, and examined for full intestines to verify that they had fed. For certain foods (egg yolk, artemia, and spirulina), feeding could be determined visually by the color of the intestine. For other foods (glucose and egg white), feeding was determined by an expansion of the intestinal lumen and the presence of bile. After verifying feeding, larvae that were going to continue past the 1 h mark of the feeding time course were placed in EM and returned to the incubated shaker for the duration of their time course.

Transmission Electron Microscopy—For TEM, unfed larvae and larvae with “full” intestines were removed and fixed at different times after feeding. After two EM rinses and anesthetization using tricaine, larvae were fixed in a 3% glutaraldehyde, 1% formaldehyde, 0.1 M cacodylate solution for 1–3 h. Heads and tails were trimmed, and swim bladders were deflated before embedding in 2% low melt agarose. Postfixation was done in 1% osmium tetroxide + 1% potassium ferricyanide in cacodylate solution for 1 h. This was followed by washes in water, cacodylate, and water again (2 × 10 min each) and then incubation in 0.05 M maleate, pH 6.5, for 10 min. Samples were then stained en bloc with 0.5% uranyl acetate in maleate for 2 h at room temperature or at 4 °C overnight. After two 15-min washes with water, samples were dehydrated through graded ethanol dilution (35%, 2 × 15 min; 50%, 15 min; 75%, 15 min; 95%, 15 min; 100%, 3 × 15 min). Samples were then washed with propylene oxide three times before incubation in 1:1 propylene oxide/resin (Epon 812 epoxy) and evaporated overnight, followed by two 2-h washes in 100% resin and a final embedding in 100% resin at 50 °C followed by 70 °C. Sections were made with a Reichert Ultracut-S (Leica Microsystems), mounted on naked 200 thin mesh grids, and stained with lead citrate. Images were captured with a Phillips Tecnai 12 microscope and recorded with a Gatan multiscan CCD camera using Digital Micrograph software.

Drug Treatments—For all treatments, vehicle or drug was added to the 5% egg yolk emulsions directly after sonication, before vortexing. For orlistat treatment, larvae were pretreated 1 h before feeding with 0.5 mM orlistat (Alli, 60-mg capsules, GlaxoSmithKline), 0.1% ethanol in EM and then fed a high-fat meal containing orlistat (0.5 mM orlistat, 0.1% ethanol, 5% egg yolk emulsion in EM). For ezetimibe (SCH58053, Santa Cruz Biotechnology) treatment, larvae were pretreated overnight with vehicle (0.1% ethanol in EM) or drug (5 μM ezetimibe, 0.1% ethanol in EM). Larvae were fed the high-fat meal containing either vehicle (0.2% ethanol, 5% egg yolk emulsion in EM) or drug (10 μM ezetimibe, 0.2% ethanol, 5% egg yolk emulsion in EM). For MTP inhibitor (AEGR-773, Aegerion Pharmaceuticals) treatment, larvae were pretreated 1 h before feeding with

vehicle (0.1% ethanol, EM) or drug (10 μ M MTP inhibitor, 0.1% ethanol in EM). Larvae were fed a high-fat meal following the procedures outlined above, with two additional experimental groups: high-fat meal plus vehicle (0.1% ethanol, 5% egg yolk emulsion in EM) and a high-fat meal plus drug (10 μ M MTP inhibitor, 0.1% ethanol, 5% egg yolk emulsion in EM).

Quantification of Coefficient of Variation of Nuclear Curvature in Electron Micrographs—To define the curvature of nuclei under different feeding conditions and drug treatments, data were collected from several sets of larvae from at least two independent experiments per condition examined. TEM images of a complete transverse section of a larval intestine were divided into four equal quadrants, and one quadrant was randomly selected for further analysis. Random quadrant selection was automated using MetaMorph software (Molecular Devices, LLC). Nuclei in the selected quadrant were then segmented by hand with the aid of a Wacom Intuos4 tablet (Wacom Technology Corp.). The experimental condition of the images was blinded for the analyses in Fig. 1. Nuclear outlines were binarized (MetaMorph) and then analyzed for curvature with a custom algorithm implemented in MATLAB (The Mathworks) using the Image Processing toolbox, as follows. The starting point is a segmented image of the nucleus. The command “bwboundaries” was used to obtain the boundary of the segmented nucleus, using the default 8-connected neighborhood. This leads to a set of pixels,

$$z_i = (x_i, y_i), \quad i = 1, \dots, n \quad (\text{Eq. 1})$$

where n is the number of pixels in the boundary. For each of these points, we then did the following. 1) We found the osculating circle at z_i along the boundary, by calculating the radius, r_i , and the center, c_i . To compute the radius and center that define the osculating circle at index i , we took $\sim 5\%$ of the pixels on the boundary before and after index i ,

$$\bar{Z}_i = \left\{ \underbrace{z_{i-m}, z_{i-m+1}, \dots, z_{i-1}}_{m \text{ pixels}}, z_i, \underbrace{z_{i+1}, \dots, z_{i+m-1}, z_{i+m}}_{m \text{ pixels}} \right\} \quad (\text{Eq. 2})$$

where $m = n/20$. We fit the circle to these $2m + 1$ points by minimizing the geometric error (sum of squared distances from the points to the fitted circle) using nonlinear least squares. This is based on the work of Gander *et al.* (55) and uses the implementation “fitcircle,” available from MATLAB Central file exchange (56). We computed the magnitude of the curvature at z_i as the inverse of the radius, $\kappa_i = 1/r_i$. If the computed radius is infinite (NaN) then the curvature was set to be zero; otherwise, we took the inverse of the radius. 2) We set the sign of the curvature by determining whether the center of the osculating circle was inside or outside the cell boundary. To this end, we computed a short line from the point z_i in the direction of the circle center c_i . This cannot be too long, or it might go through the boundary on the other side of the cell. We used lines 3 pixels long. If this point is inside the cell, then the curvature is negative; otherwise, it is positive.

After these calculations, we had a set of local curvatures $\{\kappa_i\}_{i=1}^n$ at each of the points along the boundary. Finally, we computed the mean

$$\mu(\kappa) = \frac{1}{n} \sum_i \kappa_i, \quad (\text{Eq. 3})$$

S.D. value,

$$\sigma(\kappa) = \left(\frac{1}{n-1} \sum_i (\kappa_i - \mu(\kappa))^2 \right)^{1/2}, \quad (\text{Eq. 4})$$

and coefficient of variation of the local curvatures.

$$c_v = \frac{\sigma(\kappa)}{\mu(\kappa)} \quad (\text{Eq. 5})$$

This presents a measure of the variation of local curvature around the mean. Note that for a perfectly round cell, the S.D. is zero, and hence so is c_v . Normalization for the mean allows us to compare nuclei of varying size.

RNA Extraction from Larval Guts—A feeding time course was undertaken with 6.5-dpf larval zebrafish. 5% egg yolk emulsion (high-fat) feeds and 10% egg white feeds were prepared as described above. At the appropriate time points, digestive organs (intestine, liver, and pancreas) were dissected from 10 anesthetized larval zebrafish and immediately transferred into 30 μ l of RNALater (Ambion). The samples were stored at -20°C and thawed on ice, and RNA was extracted using an RNAqueous-Micro kit (Ambion) and stored at -80°C .

RNA-seq Sample Preparation and Analysis—Triplicate samples were independently prepared from pairwise crosses fed each food type. RNA sample purity was verified with the Agilent RNA 6000 Pico kit and an Agilent 2100 bioanalyzer (Agilent Technologies). cDNA libraries were constructed from poly(A)-selected RNA using the Illumina TruSeq RNA Sample Prep kit version 2 (Illumina) following the LS (low sample throughput) option. Six samples were run per lane on an Illumina HiSeq2000 system for a 50-bp plus indexing run. Refseq annotation for zebrafish was obtained from Ensembl. RNA-seq reads were mapped to the zebrafish genome (Zv9) by Tophat (57) using the Refseq annotation as a reference. All reads were trimmed to 50 bp before mapping. Reads falling on each gene were counted using custom scripts. Differentially expressed genes were called using edgeR (58).

RT-PCR Sample Preparation and Analysis—Guts were collected from 10 larvae per experimental group and pooled together. Samples were collected in triplicate, each from a different AB cross. cDNA was constructed from RNA extracted from dissected larval guts with the iScript cDNA synthesis kit (Bio-Rad). Triplicate RT-PCR samples were prepared using cDNA, SsoAdvanced Universal SYBR Green Supermix (Bio-Rad), and gene-specific primers. The Bio-Rad CFX96.5 real-time system was used to run the RT-PCR, with 45 cycles: 95°C for 15 s, 59°C for 20 s, and 72°C for 20 s. The Bio-Rad CFX Manager version 3.0 software platform was used to analyze the results. Gene expression was quantified using the $\Delta\Delta\text{CT}$ method (59, 60) using 18S as the reference gene. The following apolipoprotein and 18S primer sequences were developed and validated in a previous publication (36): apoA-IVa, GACCCA-GCTCAAGCCTTATG (forward) and GACCCAGCTCAAG-

CCTTATG (reverse); apoA-IVb.1, GAGTTCCAGAAAACCTGTGAGTCCTCTAGCT (forward) and TCGTACAGAGAGATCAGCTGGTCTTTTAGG (reverse); apoA-IVb.2, TTGTGGTCTTTGCACTTGCT (forward) and TCATCTTGACGGTTTCCTCTG (reverse); apoA-IVb.3, TGAAGGTTCTTGTTGTGCTC (forward) and AATGGATTCTCTGCGGTTT (reverse); apoA-Ia, CCAATTTGTTCCAGGCTGAT (forward) and CAACTGGGTGGAGATGGTCT (reverse); apoEa, GCAAACTCTGATGAGCTCAAGAACAAAGC (forward) and AAGTAAGGCTCCAGACGATCCTTCACATCT (reverse); apoBa, TGACCTCAAGCACGTCACTC (forward) and GGGGAAAACCAGCACTTGTA (reverse); apoBb.1, GCTTGAAAGGAACCAGCAGTC (forward) and AGTTGGTGGTTGGCATTAGC (reverse); rps18, TGCAGAACCCTCGCCAGTACAAAATCCCAG (forward) and CCAGAAGTGACGGAGACACGGTGAGCCCT (reverse). Additional primer sequences were as follows: acot, CATGTGAATGAGGATAACCATGT (forward) and TCAACAGAAGCCCAGTTCTGA (reverse); creb3l3a, AAGCCCTTCACAGACACCAA (forward) and GAGTACGGATGGTCGAGGTT (reverse); elolv5, AATGGCTGGCTGTATTTC (forward) and TGGCCGTTTACTGATCCATT (reverse); hmgs1, GCTGAGACAATGAAGCTCAGA (forward) and CATGGATCGTCTGGCATACT (reverse); plin2, TTCATAATGGGCTGGAAGA (forward) and CACCACACATGTGCTCTGAA (reverse); MTP, GAGGCCACGCTGGACTTCAT (forward) and TTGGACACCGTCTCTCTGAAG (reverse).

Statistics—Unless otherwise indicated, one-way ANOVA with significance set at $p < 0.05$ was used to compare differences between experimental conditions after determining homogeneity of variances across samples using Bartlett's test. Tukey's multiple comparison test was used for post-hoc analysis. Results of the multiple comparison tests are indicated by *letters* (significant differences between conditions fell into families) or *asterisks*, depending on the experimental results. All *error bars* represent S.D. The GraphPad Prism software platform was used to compile all statistical analyses (GraphPad Prism version 6.0b for Mac, GraphPad Software).

Author Contributions—E. M. Z. was the lead author and was responsible for the primary experimental design and analysis. M. H. W. performed some RT-PCR and data analysis and contributed to the writing and editing of the manuscript. X. Z. performed RNA-seq analysis. P. A. I. designed, wrote, and optimized the Matlab curvature script. M. A. Sepanski designed TEM methodology, preparation, and imaging. M. A. Siddiqi designed and wrote two metamorph journals to complement the Matlab script. J. L. A. assisted with statistical analysis and assisted with editing the manuscript. Y. Z. provided expertise and guidance with experimental design and provided editorial assistance with the manuscript. S. A. F. oversaw all aspects of the experiments, provided advice on experimental design, and wrote the manuscript with E. M. Z.

Acknowledgments—We thank Joseph Tran and Matthew Sieber for helpful discussion and technical advice.

References

1. Creamer, B. (1974) Intestinal structure in relation to absorption. *Biomembranes* **4A**, 1–42

2. Buschmann, R. J., and Manke, D. J. (1981) Morphometric analysis of the membranes and organelles of small intestinal enterocytes. II. Lipid-fed hamster. *J. Ultrastruct. Res.* **76**, 15–26
3. Buschmann, R. J., and Manke, D. J. (1981) Morphometric analysis of the membranes and organelles of small intestinal enterocytes. I. Fasted hamster. *J. Ultrastruct. Res.* **76**, 1–14
4. Anderson, J. L., Carten, J. D., and Farber, S. A. (2011) Zebrafish lipid metabolism: from mediating early patterning to the metabolism of dietary fat and cholesterol. *Methods Cell Biol.* **101**, 111–141
5. Asaoka, Y., Terai, S., Sakaida, I., and Nishina, H. (2013) The expanding role of fish models in understanding non-alcoholic fatty liver disease. *Dis. Model. Mech.* **6**, 905–914
6. Fang, L., Liu, C., and Miller, Y. I. (2014) Zebrafish models of dyslipidemia: relevance to atherosclerosis and angiogenesis. *Transl. Res.* **163**, 99–108
7. Hölttä-Vuori, M., Salo, V. T., Nyberg, L., Brackmann, C., Enejder, A., Panula, P., and Ikonen, E. (2010) Zebrafish: gaining popularity in lipid research. *Biochem. J.* **429**, 235–242
8. Schlegel, A., and Stainier, D. Y. (2007) Lessons from “lower” organisms: what worms, flies, and zebrafish can teach us about human energy metabolism. *PLoS Genet.* **3**, e199
9. Farber, S. A., Pack, M., Ho, S. Y., Johnson, I. D., Wagner, D. S., Dosch, R., Mullins, M. C., Hendrickson, H. S., Hendrickson, E. K., and Halpern, M. E. (2001) Genetic analysis of digestive physiology using fluorescent phospholipid reporters. *Science* **292**, 1385–1388
10. Hama, K., Provost, E., Baranowski, T. C., Rubinstein, A. L., Anderson, J. L., Leach, S. D., and Farber, S. A. (2009) *In vivo* imaging of zebrafish digestive organ function using multiple quenched fluorescent reporters. *Am. J. Physiol. Gastrointest. Liver Physiol.* **296**, G445–G453
11. Clifton, J. D., Lucumi, E., Myers, M. C., Napper, A., Hama, K., Farber, S. A., Smith A. B., 3rd, Huryn, D. M., Diamond, S. L., and Pack, M. (2010) Identification of novel inhibitors of dietary lipid absorption using zebrafish. *PLoS One* **5**, e12386
12. Carten, J. D., Bradford, M. K., and Farber, S. A. (2011) Visualizing digestive organ morphology and function using differential fatty acid metabolism in live zebrafish. *Dev. Biol.* **360**, 276–285
13. Webster, M., Witkin, K. L., and Cohen-Fix, O. (2009) Sizing up the nucleus: nuclear shape, size and nuclear-envelope assembly. *J. Cell Sci.* **122**, 1477–1486
14. Worman, H. J., Ostlund, C., and Wang, Y. (2010) Diseases of the nuclear envelope. *Cold Spring Harb. Perspect. Biol.* **2**, a000760
15. Queisser, G., Wiegert, S., and Bading, H. (2011) Structural dynamics of the cell nucleus: basis for morphology modulation of nuclear calcium signaling and gene transcription. *Nucleus* **2**, 98–104
16. Murphy, S., Martin, S., and Parton, R. G. (2009) Lipid droplet-organelle interactions: sharing the fats. *Biochim. Biophys. Acta* **1791**, 441–447
17. Wallace, K. N., Akhter, S., Smith, E. M., Lorent, K., and Pack, M. (2005) Intestinal growth and differentiation in zebrafish. *Mech. Dev.* **122**, 157–173
18. Stoekenius, W., and Mahr, S. C. (1965) Studies on the reaction of osmium tetroxide with lipids and related compounds. *Lab. Invest.* **14**, 1196–1207
19. Skellon, J. H., and Windsor, D. A. (1962) The fatty acid composition of egg yolk lipids in relation to dietary fats. *J. Sci. Food Agric.* **13**, 300–303
20. Chakraborty, R. D., Chakraborty, K., and Radhakrishnan, E. V. (2007) Variation in fatty acid composition of *Artemia salina* nauplii enriched with microalgae and baker's yeast for use in larviculture. *J. Agric. Food Chem.* **55**, 4043–4051
21. Husbands, D. R. (1970) The composition of triglycerides from liver, egg yolk and adipose tissue of the laying hen. *Biochem. J.* **120**, 365–371
22. Jones, D. (1969) Variations in the cholesterol content of egg yolk. *Nature* **221**, 780
23. van Heek, M., Austin, T. M., Farley, C., Cook, J. A., Tetzloff, G. G., and Davis, H. R. (2001) Ezetimibe, a potent cholesterol absorption inhibitor, normalizes combined dyslipidemia in obese hyperinsulinemic hamsters. *Diabetes* **50**, 1330–1335
24. Altmann, S. W., Davis, H. R., Jr., Zhu, L. J., Yao, X., Hoos, L. M., Tetzloff, G., Iyer, S. P., Maguire, M., Golovko, A., Zeng, M., Wang, L., Murgolo, N., and Graziano, M. P. (2004) Niemann-Pick C1 Like 1 protein is critical for intestinal cholesterol absorption. *Science* **303**, 1201–1204

25. Garcia-Calvo, M., Lisnock, J., Bull, H. G., Hawes, B. E., Burnett, D. A., Braun, M. P., Crona, J. H., Davis, H. R., Jr., Dean, D. C., Detmers, P. A., Graziano, M. P., Hughes, M., Macintyre, D. E., Ogawa, A., O'Neill, K. A., *et al.* (2005) The target of ezetimibe is Niemann-Pick C1-Like 1 (NPC1L1). *Proc. Natl. Acad. Sci. U.S.A.* **102**, 8132–8137
26. Baek, J. S., Fang, L., Li, A. C., and Miller, Y. I. (2012) Ezetimibe and simvastatin reduce cholesterol levels in zebrafish larvae fed a high-cholesterol diet. *Cholesterol* **2012**, 564705
27. Hogan, S., Fleury, A., Hadvary, P., Lengsfeld, H., Meier, M. K., Triscari, J., and Sullivan, A. C. (1987) Studies on the antiobesity activity of tetrahydrolipstatin, a potent and selective inhibitor of pancreatic lipase. *Int. J. Obes.* **11**, 35–42
28. Farese, R. V., Jr., and Walther, T. C. (2009) Lipid droplets finally get a little R-E-S-P-E-C-T. *Cell* **139**, 855–860
29. Sturley, S. L., and Hussain, M. M. (2012) Lipid droplet formation on opposing sides of the endoplasmic reticulum. *J. Lipid Res.* **53**, 1800–1810
30. Otis, J. P., Zeituni, E. M., Thierier, J. H., Anderson, J. L., Brown, A. C., Boehm, E. D., Cerchione, D. M., Ceasrine, A. M., Avraham-Davidi, I., Tempelhof, H., Yaniv, K., and Farber, S. A. (2015) Zebrafish as a model for apolipoprotein biology: comprehensive expression analysis and a role for apoA-IV in regulating food intake. *Dis. Model. Mech.* **8**, 295–309
31. Iqbal, J., and Hussain, M. M. (2009) Intestinal lipid absorption. *Am. J. Physiol. Endocrinol. Metab.* **296**, E1183–E1194
32. Cuchel, M., Bloedon, L. T., Szapary, P. O., Kolansky, D. M., Wolfe, M. L., Sarkis, A., Millar, J. S., Ikewaki, K., Siegelman, E. S., Gregg, R. E., and Rader, D. J. (2007) Inhibition of microsomal triglyceride transfer protein in familial hypercholesterolemia. *N. Engl. J. Med.* **356**, 148–156
33. Robl, J. A., Sulsky, R., Sun, C. Q., Simpkins, L. M., Wang, T., Dickson, J. K., Jr., Chen, Y., Magnin, D. R., Taunk, P., Slusarchyk, W. A., Biller, S. A., Lan, S. J., Connolly, F., Kunselman, L. K., and Sabrah, T. (2001) A novel series of highly potent benzimidazole-based microsomal triglyceride transfer protein inhibitors. *J. Med. Chem.* **44**, 851–856
34. Cardell, R. R., Jr., Badenhansen, S., and Porter, K. R. (1967) Intestinal triglyceride absorption in the rat: an electron microscopical study. *J. Cell Biol.* **34**, 123–155
35. Jersild, R. A., Jr. (1966) A time sequence study of fat absorption in the rat jejunum. *Am. J. Anat.* **118**, 135–162
36. Palay, S. L., and Karlin, L. J. (1959) An electron microscopic study of the intestinal villus. II. The pathway of fat absorption. *J. Biophys. Biochem. Cytol.* **5**, 373–384
37. Jasper, D. K., and Bronk, J. R. (1968) Studies on the physiological and structural characteristics of rat intestinal mucosa: mitochondrial structural changes during amino acid absorption. *J. Cell Biol.* **38**, 277–291
38. Mishra, P., and Chan, D. C. (2016) Metabolic regulation of mitochondrial dynamics. *J. Cell Biol.* **212**, 379–387
39. Boström, P., Rutberg, M., Ericsson, J., Holmdahl, P., Andersson, L., Frohman, M. A., Borén, J., and Olofsson, S. O. (2005) Cytosolic lipid droplets increase in size by microtubule-dependent complex formation. *Arterioscler. Thromb. Vasc. Biol.* **25**, 1945–1951
40. Bouma, M. E., Beucler, I., Pessah, M., Heinzmann, C., Lusi, A. J., Naim, H. Y., Ducastelle, T., Leluyer, B., Schmitz, J., and Infante, R. (1990) Description of two different patients with abetalipoproteinemia: synthesis of a normal-sized apolipoprotein B-48 in intestinal organ culture. *J. Lipid Res.* **31**, 1–15
41. Hamilton, R. L., Wong, J. S., Cham, C. M., Nielsen, L. B., and Young, S. G. (1998) Chylomicron-sized lipid particles are formed in the setting of apolipoprotein B deficiency. *J. Lipid Res.* **39**, 1543–1557
42. Zhang, C., Wang, G., Zheng, Z., Maddipati, K. R., Zhang, X., Dyson, G., Williams, P., Duncan, S. A., Kaufman, R. J., and Zhang, K. (2012) Endoplasmic reticulum-tethered transcription factor cAMP responsive element-binding protein, hepatocyte specific, regulates hepatic lipogenesis, fatty acid oxidation, and lipolysis upon metabolic stress in mice. *Hepatology* **55**, 1070–1082
43. Lee, J. H., Giannikopoulos, P., Duncan, S. A., Wang, J., Johansen, C. T., Brown, J. D., Plutzky, J., Hegele, R. A., Glimcher, L. H., and Lee, A. H. (2011) The transcription factor cyclic AMP-responsive element-binding protein H regulates triglyceride metabolism. *Nat. Med.* **17**, 812–815
44. Omori, Y., Imai, J., Watanabe, M., Komatsu, T., Suzuki, Y., Kataoka, K., Watanabe, S., Tanigami, A., and Sugano, S. (2001) CREB-H: a novel mammalian transcription factor belonging to the CREB/ATF family and functioning via the box-B element with a liver-specific expression. *Nucleic Acids Res.* **29**, 2154–2162
45. Zhang, K., Shen, X., Wu, J., Sakaki, K., Saunders, T., Rutkowski, D. T., Back, S. H., and Kaufman, R. J. (2006) Endoplasmic reticulum stress activates cleavage of CREBH to induce a systemic inflammatory response. *Cell* **124**, 587–599
46. Thisse, B., and Thisse, C. (2004) Fast release clones: a high throughput expression analysis. ZFIN Direct Data Submission
47. Barbosa, S., Fasanella, G., Carreira, S., Llerena, M., Fox, R., Barreca, C., Andrew, D., and O'Hare, P. (2013) An orchestrated program regulating secretory pathway genes and cargos by the transmembrane transcription factor CREB-H. *Traffic* **14**, 382–398
48. Weinberg, R. B., Gallagher, J. W., Fabritius, M. A., and Shelness, G. S. (2012) ApoA-IV modulates the secretory trafficking of apoB and the size of triglyceride-rich lipoproteins. *J. Lipid Res.* **53**, 736–743
49. Karathanasis, S. K., Yunis, I., and Zannis, V. I. (1986) Structure, evolution, and tissue-specific synthesis of human apolipoprotein AIV. *Biochemistry* **25**, 3962–3970
50. Elshourbagy, N. A., Walker, D. W., Boguski, M. S., Gordon, J. I., and Taylor, J. M. (1986) The nucleotide and derived amino acid sequence of human apolipoprotein A-IV mRNA and the close linkage of its gene to the genes of apolipoproteins A-I and C-III. *J. Biol. Chem.* **261**, 1998–2002
51. VerHague, M. A., Cheng, D., Weinberg, R. B., and Shelness, G. S. (2013) Apolipoprotein A-IV expression in mouse liver enhances triglyceride secretion and reduces hepatic lipid content by promoting very low density lipoprotein particle expansion. *Arterioscler. Thromb. Vasc. Biol.* **33**, 2501–2508
52. Cheng, D., Xu, X., Simon, T., Boudyguina, E., Deng, Z., VerHague, M., Lord, C., Brown, J. M., Lee, A. H., Shelness, G. S., Weinberg, R. B., and Parks, J. S. (2016) Very low density lipoprotein assembly is required for cAMP-responsive element-binding protein H processing and hepatic apolipoprotein A-IV expression. *J. Biol. Chem.* **291**, 23793–23803
53. Westerfield, M. (1995) *The Zebrafish Book*, 3rd Ed., University of Oregon, Eugene, OR
54. Semova, I., Carten, J. D., Stombaugh, J., Mackey, L. C., Knight, R., Farber, S. A., and Rawls, J. F. (2012) Microbiota regulate intestinal absorption and metabolism of Fatty acids in the zebrafish. *Cell Host Microbe* **12**, 277–288
55. Gander, W., Golub, G. H., and Strebel, R. (1994) Least-squares fitting of circles and ellipses. *BIT* **34**, 558–578
56. Brown, R. (2007) fitcircle.m, Matlab Central: File Exchange
57. Kim, D., Pertea, G., Trapnell, C., Pimentel, H., Kelley, R., and Salzberg, S. L. (2013) TopHat2: accurate alignment of transcriptomes in the presence of insertions, deletions and gene fusions. *Genome Biol.* **14**, R36
58. Robinson, M. D., McCarthy, D. J., and Smyth, G. K. (2010) edgeR: a bioconductor package for differential expression analysis of digital gene expression data. *Bioinformatics* **26**, 139–140
59. Schmittgen, T. D., and Livak, K. J. (2008) Analyzing real-time PCR data by the comparative $C(T)$ method. *Nat. Protoc.* **3**, 1101–1108
60. Livak, K. J., and Schmittgen, T. D. (2001) Analysis of relative gene expression data using real-time quantitative PCR and the $2(-\Delta\Delta C(T))$ method. *Methods* **25**, 402–408